ACADEMIA JOURNAL OF BIOLOGY 2025, 47(3): 115–128
DOI: 10.15625/2615-9023/22091

IDENTIFICATION OF RESISTANCE-MODIFYING AGENTS FROM *Pteris vittata* L. BY UNTARGETED METABOLOMIC ANALYSIS AND IN SILICO SCREENING

Nguyen Phuong Nhung, Dao Yen Vy, Nguyen Thi Thao Ngan, Nguyen Thi Kieu Oanh*

Department of Life Sciences, University of Science and Technology of Hanoi, Vietnam
Academy of Science and Technology, 18 Hoang Quoc Viet, Ha Noi, Vietnam

Received 18 December 2024; accepted 18 September 2025

ABSTRACT

Antibiotic resistance is becoming an urgent public health concern worldwide, which leads to the urgent need for research and development of new antibacterials or new resistance-modifying agents. *Pteris vittata* L., which belongs to the Pteridaceae family, is a hyperaccumulator plant growing in metalliferous soils. This harsh environment is supposed to induce the expression or the dispersion of multidrug-resistant phenotypes through the action of efflux pumps in bacterial membranes to exclude heavy metals. Previous studies showed the potential inhibition of *P. vittata* extracts on *Stenophomonas maltophilia* isolates. Therefore, to identify the active compounds in the plant, the whole metabolome of *P. vittata* was screened by untargeted analysis using the LC-MS-qToF system and then applied virtual docking to investigate the interaction of these compounds on an efflux pump model. Over one hundred compounds extracted from the root and leaf samples were docked on the SmeDEF protein using the Autodock Vina 4.2.6 application. As a preliminary result, we suggested nine flavonoid compounds showing the most negative binding energies with the chosen protein for further *in vitro* experimental confirmation.

Keywords: antibiotic resistance, in silico screening, UPLC-QToFMS, *Pteris vittata*, RND efflux pump, SmeDEF.

Citation: Nguyen Phuong Nhung, Dao Yen Vy, Nguyen Thi Thao Ngan, Nguyen Thi Kieu Oanh, 2025. Identification of resistance-modifying agents from *Pteris vittata* L. By untargeted metabolomic analysis and in silico screening. *Academia Journal of Biology*, 47(3): 115–128. https://doi.org/10.15625/2615-9023/22091

**Corresponding author email*: nguyen-thi-kieu.oanh@usth.edu.vn

INTRODUCTION

Antimicrobial resistance is currently a global threat that requires emergency action to achieve and maintain the sustainable development of the whole world. This happens when pathogens (such as bacteria, fungi, viruses, and parasites) can develop over time and can resist drug treatment effects at a certain level. Both misuse and overuse of antibiotic drugs in human, veterinary, and agricultural activities might lead to the growth of multidrug-resistant pathogens (Mittal et al., 2020). There were many other pressures that co-select for resistance to antibiotics, including metals, pollutants, hydrocarbons, biocides, pesticides, etc. The alarming multidrug resistance conditions might affect the economy since the longer it took for patients to recover or prolonged ailments, the need for expensive medicines rises, longer hospital continuance, and more financial provocations were affected. In the modern medical field, the deficiency of antibiotics is a major difficulty since it could increase the risks of significant surgery, cancer treatment, or microbial infection. It leads to an urgent need for the discovery of new antibacterial or new resistance-modifying agents that can respectively directly inhibit the growth of bacteria or alter the resistant phenotypes of the host organisms.

Pteris vittata L. is well-known as a Chinese brake fern and belongs to the Pteridaceae family. This species is confirmed to have originated natively in tropical and subtropical habitats. In Vietnam, the native environment for the natural growth of this species could be observed in metalliferous mining sites in Thai Nguyen province (Nguyen et al., 2021). It has a considerable ability to discard the excess amount of arsenic (As) from the soil to enhance the rapid growth even in the polluted habitat through the large biological mass and expanded root system (Cesaro, 2015). Our previous study has shown the targeted metabolite profiles of *P. vittata* based on a widely targeted metabolomics approach (Nguyen et al., 2022). This method has been robust in terms of structural elucidation level; however, the identification was determined only in a list of compounds in the home library, not yet reach to compounds that do not belong to the collection. One of the aims of our study is to expand the database of promising compounds in this plant with an untargeted strategy using high-resolution mass spectrometry.

Our screening data showed that the crude extract of *P. vittata* demonstrated potential activity against some bacterial strains of *Stenotrophomonas maltophilia*, such as K279a, 0366. These isolates were well-known as non-selective multidrug-resistant bacteria because of the presence of efflux pumps (Youenou et al., 2015; Alonso & Martinez, 2001). Efflux pumps were known for the complete transport systems, including heavy metal ions (cations & anions), xenobiotics, hydrophobic and amphiphilic compounds, and most importantly, drugs. The resistance-nodulation-division (RND) family firstly contains many amino acid residues within, and composes of two homologous subunits, the drugs could be pumped through these efflux pumps in bacterial cells. RND efflux pumps are located in the bacterial cell membrane, using the transport mechanism to lower the concentration of the drugs, such as antibiotics, within the cell, thereby leading to the resistance ability to bacteria (Ling et al., 2016). Their majority is distinctly ascertained in Gram-negative bacteria, but they also exist in Gram-positive archaea and eukaryotes. They could be found in cytoplasmic membranes to facilitate substrate transportation within the cell (Colclough et al., 2020). Secondly, these RND systems take charge of the maintenance of cell homeostasis deletion of toxins hence leading to drug resistance in bacteria once they get over-expressed before the drug could be activated. SmeDEF is a multidrug RND pump protein that has been found in *S. maltophilia*, and its overexpression was just to some antibiotics (Wu et al., 2019). This protein belongs to the multidrug efflux pump structure in the bacteria *S. maltophilia* and is involved in bacterial resistance to different antimicrobial agents (Sánchez et al., 2016). Normally, the efflux pump system is used in bacteria to removal the

toxins, harmful substances for bacterial growth, including antibiotics. The energy within the bacterial cell assists the transportation of the pump system through the cell membrane to the outer of the cells.

In this study, we examined the potential of *P. vittata* metabolites revealed by untargeted analysis on the interaction with the SmeDEF protein. Prediction was given on the correlation between the antimicrobial characteristics of the compounds in *P. vittata* with the mechanism of the RND efflux pump on the SmeDEF protein.

MATERIALS AND METHODS

Materials

P. vittata samples were collected in Hich village, Tan Long, Dong Hy, Thai Nguyen province, Vietnam (21°43'57"N; 105°51'25"E) on June 30th, 2022, then identified by Dr. Nguyen The Cuong, Institute of Biology, Vietnam Academy of Science and Technology (VAST). A voucher of specimen was deposited at the Department of Life Sciences, University of Science and Technology of Hanoi, VAST, 18 Hoang Quoc Viet, Cau Giay, Ha Noi, Vietnam.

For sample treatment, roots and leaves were separated and labelled as RPV for root samples and LPV for leaf samples. The plant samples were dried in an oven at 45 °C for 48 hours until they were fully dehydrated. Consequently, these materials were ground using a Mixer Mill MM 400 (Restch, Germany). Afterward, they were desiccated and divided into falcons for storage at -80 °C.

Methods

Sample extraction

Approximately 50 mg of leaf and root powders were weighed into a tube. After adding 5 mL of 80% methanol (v/v) (MeOH), the extraction process was put under ultrasonic for 15 minutes with the temperature maintained around 70 °C. The extracts were then centrifuged and filtered through 0.22 µm membrane into the vials before injecting to the LCMS system.

Untargeted analysis

In this study, the untargeted analysis was performed by using ultra performance liquid chromatography (UPLC) coupled to mass spectrometry with a detector quadrupole time of flight (MS-QToF). In which the chromatographic dissociation was carried out on an ACQUITY UPLC BEH C18 column (130 A°, 1.7 µm, 2.1 mm x 100 mm), applied a gradient elution of mobile phase including solutions A (water and 0.1% formic acid) and B (MeOH). The running method began at 0.5 minutes with 99% of solution A, then decreased to 65% of solution A during the next 15.5 minutes and finally maintained at 0% of solution A for 2 minutes. The column took 5 more minutes to re-equilibrate to 99% of solution A before starting the next turn. During the running time of a turn, the flow rate stayed stable at 0.3 mL/min. Each sample was injected with 1 µL.

For the QToF detection, the analysis was acquired on MSe mode to get accurate full scan identified elements and quality counts from 100 to 1,500 m/z, at a rate of 1 scan per 0.1 second. Each sample was ionized in both positive and negative ionization modes. In addition, each scan was recorded at high energy and low energy conditions, which allows us to observe molecular ions and their fragments. The cone voltage was 6V and the collision energy went up from 15 to 40 V. Overall values involved: capillary voltage was 2.00 kV, the sample cone voltage was 100 V, source temperature was 120 °C, desolvation temperature was 550 °C, cone gas was 30 L/h, and desolvation was 1000 L/h.

The acquisition was controlled by Masslynx 4.2 (Waters Coproration) and the processing of the obtained raw files was conducted in UNIFY software (Waters Coproration). All peaks detected by the intensity threshold at 10,000 counts and their mass error under 5 ppm were selected for identification. The library source was from the Waters Traditional Medicine Library, which consists of more than 6300 natural products.

From the raw data, all Simplified Molecular Input Line Entry System (SMILES) files of the compounds were searched and collected by ChemSpider and PubChem. They were widely used as a performance of chemical structure in computer drug design.

Protein homology modelling

SWISS-MODEL website (https://swiss-model.expasy.org/) was exploited to build the structure of protein from the SmeDEF K279a sequence extracted from the National Library of Medicine protein database ("Protein [Internet]. Bethesda (MD): National Library of Medicine (US), National Center for Biotechnology Information; [1988]. Accession No. NM_CAG34257.1, RND protein [*Stenotrophomonas maltophilia* K279a]; [cited 2023 October 16]", 1988). We used the structure of another efflux pump (RCSB ID: 3AOD chain A) with the highest similarity (64.25%) among aligned sequences. Two bioinformatic tools, Procheck (Laskowski et al., 1993) and Molprobity (Williams et al., 2018), were applied to validate the structure of the obtained model, and the model with the most acceptable parameters was selected.

Virtual screening by molecular docking

As SmeDEF has a symmetric structure with three chains (A, B, and C), we only selected one chain (chain A) for representative docking by Discovery Studio Visualizer (Biovia et al., 2016). After that, polar hydrogen atoms as well as the Gasteiger charge field were added before converting to .pdbqt format by mgltools (ver 1.5.7) (Morris et al., 2009). A docking box was selected to cover the drug binding docking, including both distal and proximal binding regions, with the center coordinates of 164.299, 170.347, 217.271, and 35 Å in size. From the SMILES code, the structure of reference compounds, which are eight antibiotics with confirmed resistance via the SmeDEF efflux pump, including trimethoprim, erythromycin, clarithromycin, ciprofloxacin, chloramphenicol, levofloxacin, tetracycline, and sulfamethoxazole (Gil-Gil et al., 2020) and all the detected compounds in LCMS-qToF data were represented in 2D mol2 format by OpenBabel version 2.3.1 (O'Boyle et al., 2011). In the next step, the ligand library structure was imported to the PyRx tool (Dallakyan & Olson, 2015) to add polar hydrogen, adjust torsion, and convert to .pdbqt format. The binding affinity of ligands to the efflux pump was evaluated by Autodock Vina version 1.2.0 (Eberhardt et al., 2021). Exhaustiveness was changed in the range from 8 to 80. The energy range was set to 2 kcal/mol and the number of modes is 20. The docking pose with the more negative binding energy was selected.

RESULTS

Metabolome profiles of *Pteris vittata* based on LC-QTOF analysis

The UPLC-QTOF analysis revealed 99 compounds in leaf and root samples of *P. vittata*. Among all compounds detected, the data were filtered by level of response, which is the intensity of atoms that go through the detector. The results demonstrated that terpenes had the highest percentage in the *P. vittata* sample, with 48 compounds, followed by alkaloids, flavonoids, sterols, phenols and other compounds (Table 1). The summit of compounds identified in UPLC-QToF analysis was sorted out with the most important properties, including formula, expected mass (Da); mass error (mDa); observed mass (Da); Observed RT (min).

Table 1. Metabolite profiles of *Pteris vittata* extracts revealed by untargeted UPLC QToF analysis

No.	Component name	Formula	Expected mass (Da)	Mass error (mDa)	Observed mass (Da)	Observed RT (min)
1	Evocarpine	$C_{23}H_{33}NO$	339.256	-0.513	339.256	9.958
2	Withametelin C	$C_{28}H_{42}O_6$	474.298	-2.223	474.296	18.829
3	Hyperpapuanone	$C_{26}H_{38}O_4$	414.277	0.501	414.278	17.827

No.	Component name	Formula	Expected mass (Da)	Mass error (mDa)	Observed mass (Da)	Observed RT (min)
4	Angeloylgomisin Q	$C_{29}H_{38}O_9$	530.252	-1.29	530.25	20.407
5	Belladonnine	$C_{34}H_{42}N_2O_4$	542.314	-0.517	542.314	17.918
6	Oleoyl neocryptotanshinone	$C_{37}H_{54}O_5$	578.397	-2.016	578.395	18.191
7	Picrasinoside B	$C_{28}H_{40}O_{11}$	552.257	-0.22	552.257	18.165
8	Procyanidin C1	$C_{45}H_{38}O_{18}$	866.206	3.818	866.21	6.18
9	Neoxanthin	$C_{40}H_{56}O_4$	600.418	0.854	600.419	18.087
10	Esculentoside Q	$C_{47}H_{74}O_{21}$	974.472	-1.247	974.471	18.193
11	Stachysterone A	$C_{27}H_{42}O_6$	462.298	1.178	462.299	17.4
12	Phytolaccagenin	$C_{31}H_{48}O_7$	532.34	-0.914	532.339	17.845
13	Methyl 12-oxooctadec-9-enoate	$C_{19}H_{34}O_3$	310.251	0.236	310.251	17.85
14	1-Linoleoyl-3-palmitoyl-rac-glycerol	$C_{37}H_{68}O_5$	592.507	-1.278	592.505	21.047
15	Tussilagonone	$C_{21}H_{30}O_3$	330.219	-0.442	330.219	17.85
16	1,3,4,6-tetra-o-galloyl-beta-d-glucose	$C_{34}H_{28}O_{22}$	788.107	3.669	788.111	6.048
17	Isoetin	$C_{15}H_{10}O_7$	302.043	0.377	302.043	6.23
18	Sesartemin	$C_{23}H_{26}O_8$	430.163	1.415	430.164	20.29
19	Kushenol L	$C_{25}H_{28}O_7$	440.184	0.844	440.184	17.593
20	N-Methylcorydaldine	$C_{12}H_{15}NO_3$	221.105	0.869	221.106	20.929
21	Hispanolone	$C_{20}H_{30}O_3$	318.219	-0.092	318.219	17.177
22	Cornuside	$C_{24}H_{30}O_{14}$	542.164	-1.504	542.162	12.227
23	Gluroside	$C_{15}H_{24}O_8$	332.147	-1.638	332.145	17.801
24	Isotrilobine	$C_{36}H_{36}N_2O_5$	576.262	1.898	576.264	20.408
25	Villosolside	$C_{16}H_{26}O_9$	362.158	1.598	362.159	20.437
26	Diosgenin-3-O-beta-D-glucopyranoside	$C_{33}H_{52}O_8$	576.366	-2.18	576.364	18.536
27	Evobioside	$C_{35}H_{54}O_{13}$	682.356	1.056	682.357	18.052
28	1-(3,4-dimethoxyphenyl)-5-hydroxy-decan-3-one	$C_{18}H_{28}O_4$	308.199	0.657	308.199	17.696
29	Dichotomoside E	$C_{20}H_{30}O_9$	414.189	0.034	414.189	21.21
30	Embelin	$C_{17}H_{26}O_4$	294.183	0.33	294.183	15.572
31	Mahuannin A	$C_{30}H_{24}O_{10}$	544.137	0.195	544.137	6.049
32	Geissoschizine methyl ether	$C_{22}H_{26}N_2O_3$	366.194	-0.026	366.194	20.396
33	Pseudolaric acid C2	$C_{22}H_{26}O_8$	418.163	1.593	418.164	8.431
34	Pubescene A	$C_{33}H_{42}O_9$	582.283	-2.45	582.28	20.608
35	Eupatoroxin	$C_{20}H_{24}O_8$	392.147	0.549	392.148	20.522
36	Chenodeoxycholic acid	$C_{24}H_{40}O_4$	392.293	1.349	392.294	20.304
37	Rhodojaponin IV	$C_{24}H_{38}O_8$	454.257	2.167	454.259	20.4
38	Oxofangchirine	$C_{37}H_{34}N_2O_7$	618.237	-1.681	618.235	20.526
39	Cipadesin	$C_{32}H_{42}O_8$	554.288	0.915	554.289	17.823
40	Nimbolidin D	$C_{44}H_{58}O_{12}$	778.393	0.636	778.393	14.355

No.	Component name	Formula	Expected mass (Da)	Mass error (mDa)	Observed mass (Da)	Observed RT (min)
41	1-(4-Hydroxybenzyl)-4-methoxy-9,10-dihydrophenanthrene-2,7-diol	$C_{22}H_{20}O_4$	348.136	-0.803	348.135	2.933
42	Gibberellin A17	$C_{20}H_{26}O_7$	378.168	0.533	378.168	16.906
43	Neobudofficide	$C_{34}H_{42}O_{18}$	738.237	-0.792	738.236	6.043
44	Saffloquinoside B	$C_{34}H_{38}O_{17}$	718.211	-1.007	718.21	6.046
45	Saikosaponin E	$C_{42}H_{68}O_{12}$	764.471	2.571	764.474	9.953
46	Nigakihemiacetal A	$C_{22}H_{34}O_7$	410.23	1.347	410.232	20.391
47	Ginsenoside Rh2	$C_{36}H_{62}O_8$	622.444	2.81	622.447	17.832
48	Vitexifolin B	$C_{20}H_{36}O_3$	324.266	0.878	324.267	18.384
49	Javanicolide C	$C_{26}H_{36}O_{11}$	524.226	0.446	524.226	20.491
50	Danshenol B	$C_{22}H_{26}O_4$	354.183	0.047	354.183	18.06
51	Hexadecyl ferulate	$C_{26}H_{42}O_4$	418.308	418.31	1.565	17.559
52	Phanginin F	$C_{21}H_{28}O_6$	376.189	376.189	0.19	16.841
53	L-Tetrandrine	$C_{38}H_{42}N_2O_6$	622.304	622.301	-3.004	18.187
54	Apocarotenal	$C_{30}H_{40}O$	416.308	416.309	1.57	18.058
55	Stigmasteryl ferulate	$C_{39}H_{56}O_4$	588.418	588.42	1.87	17.836
56	Kansuiphorin B	$C_{54}H_{90}O_{10}$	898.653	898.658	4.274	20.555
57	Gomphrenin I	$C_{24}H_{26}N_2O_{13}$	550.143	550.146	2.378	8.551
58	Shiromodiol diacetate	$C_{19}H_{30}O_5$	338.209	338.209	-0.504	16.22
59	Curculigosaponin B	$C_{35}H_{58}O_8$	606.413	606.416	2.949	17.778
60	Ialibinone E	$C_{18}H_{24}O_4$	304.167	304.168	0.909	15.402
61	Berbamine	$C_{37}H_{40}N_2O_6$	608.289	608.286	-2.689	16.894
62	Vitamin B15	$C_{10}H_{19}NO_8$	281.111	281.11	-0.588	8.622
63	Dimethylcurcumin	$C_{23}H_{24}O_6$	396.157	396.156	-1.374	10.609
64	3-O-(2’E,4’Z-decadienoyl)ingenol	$C_{30}H_{42}O_6$	498.298	498.296	-2.241	16.098
65	Cistanoside C	$C_{30}H_{38}O_{15}$	638.221	638.222	1.189	16.026
66	Gibberellin A87	$C_{19}H_{22}O_7$	362.137	362.136	-0.161	17.131
67	Yadanzioside I	$C_{29}H_{38}O_{16}$	642.216	642.218	1.644	7.653
68	Ochrolifuanine A	$C_{29}H_{34}N_4$	438.278	438.279	0.633	16.689
69	Aspafilioside A	$C_{38}H_{62}O_{12}$	710.424	710.424	-0.023	16.126
70	Curculigosaponin C	$C_{41}H_{68}O_{13}$	768.466	768.469	3.281	16.544
71	Hymexelsin	$C_{21}H_{26}O_{13}$	486.137	486.137	-0.809	10.112
72	Digalactosyldiacylglycerol	$C_{49}H_{88}O_{15}$	916.612	916.615	2.635	17.225
73	Cristatain	$C_{36}H_{54}O_{11}$	662.367	662.364	-2.564	16.378
74	Ophiopogonin D	$C_{44}H_{70}O_{16}$	854.466	854.47	3.855	15.956
75	Vina-ginsenoside R1	$C_{44}H_{74}O_{15}$	842.503	842.501	-2.18	16.084
76	Atratoglaucoside A	$C_{34}H_{50}O_{12}$	650.33	650.333	3.216	17.86
77	Delphatine	$C_{26}H_{43}NO_7$	481.304	481.302	-1.797	20.662
78	Gingerglycolipid B	$C_{33}H_{58}O_{14}$	678.383	678.379	-3.182	16.638
79	Bruceajavanone B	$C_{39}H_{54}O_9$	666.377	666.374	-2.609	16.298

No.	Component name	Formula	Expected mass (Da)	Mass error (mDa)	Observed mass (Da)	Observed RT (min)
80	Didymin	$C_{28}H_{34}O_{14}$	594.195	594.193	-1.863	15.215
81	beta-Hederin	$C_{41}H_{66}O_{11}$	734.461	734.463	2.216	16.986
82	Forsythiaside	$C_{29}H_{36}O_{15}$	624.205	624.204	-1.766	8.518
83	Ophiopogonin B	$C_{39}H_{62}O_{12}$	722.424	722.426	1.475	16.213
84	Iristectorene B	$C_{44}H_{76}O_{5}$	684.569	684.571	1.77	12.278
85	Conyzasaponin G	$C_{41}H_{66}O_{14}$	782.445	782.448	2.451	16.101
86	Dehydrobrusatol	$C_{26}H_{30}O_{11}$	518.179	518.179	0.346	20.56
87	Norlobelanine	$C_{21}H_{23}NO_{2}$	321.173	321.174	1.008	16.354
88	Cynanchoside C2	$C_{49}H_{78}O_{15}$	906.534	906.532	-2.408	16.205
89	Beta-citraurin	$C_{30}H_{40}O_{2}$	432.303	432.303	-0.129	16.095
90	Grandoside	$C_{17}H_{32}O_{11}$	412.194	412.196	1.41	16.871
91	Adouetine X	$C_{28}H_{44}N_{4}O_{4}$	500.336	500.335	-1.233	16.677
92	Centellasaponin B	$C_{42}H_{68}O_{16}$	828.451	828.454	3.286	17.618
93	Palmitoyl arucadiol	$C_{35}H_{52}O_{4}$	536.387	536.387	-0.023	11.614
94	Platyphylline	$C_{18}H_{27}NO_{5}$	337.189	337.188	-0.663	18.217
95	Gancaonin U	$C_{24}H_{28}O_{4}$	380.199	380.199	0.372	16.85
96	16'-Decarbomethoxy-19,20-dihydroconoduramine	$C_{41}H_{52}N_{4}O_{3}$	648.404	648.405	1.019	14.56
97	Azadirachtin	$C_{35}H_{44}O_{16}$	720.263	720.266	3.309	5.521
98	Echinacoside	$C_{35}H_{46}O_{20}$	786.258	786.255	-3.558	15.938
99	Albibrissinoside A	$C_{29}H_{38}O_{17}$	658.211	658.211	0.337	10.828

Modelling of SmeDEF protein

In Figure 1, the symmetrical structure of the efflux pump was illustrated with three colors to discriminate between the three chains. The pump has a longitudinal tube with multiple accessible locations for drugs and other small molecules throughout the tube from the intracellular to extracellular domain (Yamaguchi et al., 2015). Each chain contains 12 transmembrane helices, typical of RND efflux pumps, but unlike other pumps, these helices are not divided into two groups of six between the C- and N-terminal. Instead, they are arranged in a 1–6–5 pattern. The extracellular domain has two regions: the porter and the TolC docking domain. The porter domain is further divided into subdomains between C and N terminal (PN1 and PN2 or PC1 and PC2), arranged in a β−α−β motif, while TolC docking domains include two regions denoted as DN and DC either of which has a short vertical hairpin protruding upward. Three monomers are linked by the long hairpin originating from the DN subdomain and protruding toward the DC domain of the next monomer (Yamaguchi et al., 2015). The drug-binding domain for the extracellular entrance is between PN1 and PN2, with an access pocket and a deep binding pocket split by a switch loop. While the access pocket is near the exposed region of the pump to extracellular fluid, the deep binding pocket is buried inside the pump and is very narrow in the normal state and hydrophobic. Once the protein is activated by phosphorylation, there is a transformation of the switch loop to widen the deep binding pocket and therefore facilitate the binding of the drug to SmeDEF. As antibiotics could bind to either the transmembrane or cytosolic region and "flow" to the extracellular region, an efficient efflux pump inhibitor should hinder the binding of antibiotics to the efflux pump as a competitive binding agent or allosteric inhibitor (Compagne et al., 2023).

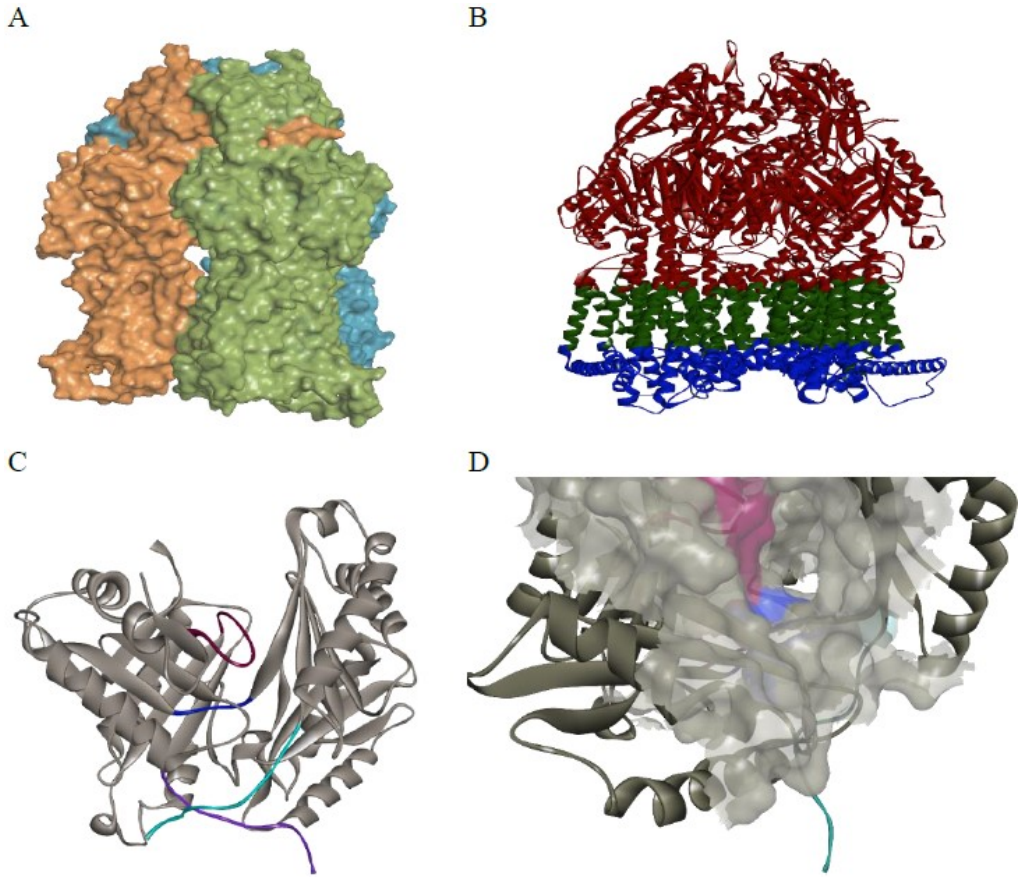

Figure 1. Structure of SmeDEF. (A) 3D SmeDEF surface. (B) SmeDEF structure: extracellular membrane (in red), transmembrane region (in green), intracellular membrane (in blue). (C) Docking region in porter domain with different loops marked by different colors, especially the switch loop in red. (D) Surface of docking pocket

In silico docking analysis

There are various types of antibiotics involved in the protein SmeDEF of *S. maltophilia*, in this study, eight antibiotics were selected as the references for the reaction between identified compounds in *P. vittata* with protein SmeDEF. They are classified into 5 classes, respectively sulfonamides (trimethoprim and sulfamethoxazole), macrolides (erythromycin and clarithromycin), quinolones or fluoroquinolones (ciprofloxacin and levofloxacin); amphenicol (chloramphenicol), and tetracyclines (tetracycline). To predict promising compounds from a large metabolome library of *P. vitatta*, all detected secondary metabolites were screened, ranked based on their binding energy, and compared to eight antibiotics. Results of reference compounds and top metabolites, which have much better binding energy than antibiotics, are exhibited inTable 2.

Among eight antibiotics, sulfamethoxazole and chloramphenicol have the lowest affinity of larger than -7 kcal/mol, while other compounds show the higher binding affinity in the range of -9 and -8 kcal/mol. The binding of antibiotics and proteins are stabilized by ionic interactions and hydrogen bonds. The obtained results are consistent with the clinical sensitivity of *S. maltophilia* to these antibiotics (Alonso & Martínez, 2000; Gil-Gil et al., 2020). Meanwhile, the energy of screened compounds considerably varies between -12 and -5 kcal/mol showing the diversity of

metabolite structure (Appendix 1). Ophiopogonin D has the strongest binding of -11.57 kcal/mol followed by nimbolidin D with -11.37 kcal/mol and saikosaponin E with -11.00 kcal/mol. Thirteen other compounds have slightly less affinity than the top three compounds of less than -10 kcal/mol. The binding modes of these metabolites overlap completely or partly with eight antibiotics, but with different types of interactions such as Van der Waals and hydrophobic interactions due to their large structures with sugar unit.

Table 2. Affinity of reference compounds (antibiotics) and top metabolites from *Pteris vittata*

No.	Compound name	Binding energy (kcal/mol)
Antibiotics		
1	Trimethoprim	-9.10
2	Tetracycline	-8.90
3	Erythromycin	-8.33
4	Levofloxacin	-8.30
5	Clarithromycin	-8.17
6	Ciprofloxacin	-7.80
7	Sulfamethoxazole	-6.70
8	Chloramphenicol	-6.50
Plant metabolites		
9	Ophiopogonin D	-11.57
10	Nimbolidin D	-11.37
11	Saikosaponin E	-11.00
12	Evobioside	-10.77
13	Procyanidin C1	-10.70
14	beta-Hederin	-10.53
15	Conyzasaponin G	-10.53
16	Aspafilioside A	-10.50
17	Cristatain	-10.47
18	Atratoglaucoside A	-10.43
19	Esculentoside Q	-10.40
20	Centellasaponin B	-10.37
21	Cynanchoside C2	-10.33
22	Neobudofficide	-10.27
23	16’-Decarbomethoxy-19,20-dihydroconoduramine	-10.20
24	Ophiopogonin B	-10.00

DISCUSSION

Although *S. maltophilia* causes severe infections in inpatients with a very high resistance rate (Ho et al., 2021; Raad et al., 2023). There have been few studies about the mechanism of antibiotic resistance, especially the structure of proteins involved, such as efflux pumps (Gil-Gil et al., 2020). SmeDEF is one of the most interesting efflux pumps, but its structure has not been resolved yet. In this study, we used homology modelling to construct the structure of the protein and anticipated the binding of secondary metabolites of *P. vittata* to the protein. Nine molecules show an extremely high affinity compared to antibiotics with the same or near binding pockets, suggesting that they could be potential inhibitors of the efflux pump, hence improving the sensitivity of eight antibiotics if they are used simultaneously with antibiotics. Although the confirmation of the mechanism of action as well as the *in vitro* activity of nine compounds should be further investigated, the

results enlighten the possibility of new drug candidates not for direct antimicrobial effect but for synergistic effect with current antibiotics.

CONCLUSION

In this study, we revealed the untargeted metabolite profile of *P. vittata* methanolic extract, including 99 compounds based on their mass exact and the similarity of mass spectrum in low and high energy modes. The *in-silico* experiment showed the link correlation between the chosen protein SmeDEF in a specific Gram-negative bacterium and the ligands that suggested the potential compounds within the plant samples. Over 99 compounds annotated in the samples and eight antibiotics as references were categorized and docked multiple times to make possible suggestions for the best match with the protein in the study. Finally, nine compounds were suggested, showing the more negative binding energy scores to advance further experimental confirmation. Further perspectives for this topic are aiming for an expanded metabolomic profile of the targeted *P. vittata* species, hence leading to a better understanding of the possibilities of interaction between the target and the receptor, to comprehend the mechanism of antimicrobial resistance in the bacteria.

Acknowledgements: This work was supported by the University of Science and Technology of Hanoi [grant number USTH.LS.01/22–24].

REFERENCES

Alonso A., Martínez J. L., 2000. Cloning and characterization of SmeDEF, a novel multidrug efflux pump from *Stenotrophomonas maltophilia*. *Antimicrob Agents Chemother*, 44(11): 3079–3086.

Alonso A., Martínez J. L., 2001. Expression of multidrug efflux pump SmeDEF by clinical isolates of *Stenotrophomonas maltophilia*. *Antimicrob Agents Chemother*, 45: 1879–1881.

Cesaro P., Cattaneo C., Bona E., Berta G., Cavaletto M., 2015. The arsenic hyperaccumulating *Pteris vittata* expresses two arsenate reductases. *Sci Rep.*, 5(1): 14525.

Colclough A. L., Alav I., Whittle E. E., Pugh H. L., Darby E. M., Legood S. W., McNeil H. E., Blair J. M. A., 2020. RND efflux pumps in Gram-negative bacteria: Regulation, structure and role in antibiotic resistance. *Future Microbiol.*, 15: 143–157. PubMed

Wu C.-J., Lu H.-F., Lin Y.-T., Zhang M.-S., Li L.-H., Yang T.-C., 2019. Substantial Contribution of SmeDEF, SmeVWX, SmQnr, and Heat Shock Response to Fluoroquinolone Resistance in Clinical Isolates of *Stenotrophomonas maltophilia*. *Front Microbiol.*, 10: 822.

Compagne N., Vieira Da Cruz A., Müller R. T., Hartkoorn R. C., Flipo M., Pos K. M., 2023. Update on the discovery of efflux pump inhibitors against critical priority Gram-negative bacteria. *Antibiotics (Basel).*, 12(1): 180.

Ling B. D., Zhang L., Li X. Z., 2016. Antimicrobial resistance and drug efflux pumps in *Acinetobacter*. In: Li X. Z., Elkins C., Zgurskaya H. (eds) *Efflux-Mediated Antimicrobial Resistance in Bacteria.* Springer: 329–358.

Gil-Gil T., Laborda P., Ochoa-Sánchez L. E., Hernando-Amado S., Martínez J. L., 2023. Efflux in Gram-negative bacteria: what are the latest opportunities for drug discovery. *Expert Opin Drug Discov.*, 18(6): 671–686.

Ho M.-C., Hsiao C.-H., Sun M.-H., Chen C.-L., Ma D.-H., Lin K.-K., Tan H.-Y., Yeh L.-K., Chang C.-J., Huang Y.-C., 2021. Antimicrobial susceptibility, minimum inhibitory concentrations, and clinical profiles of *Stenotrophomonas maltophilia* endophthalmitis. *Microorganisms*, 9(9): 1840.

Laskowski R. A., MacArthur M. W., Moss D. S., Thornton J. M., 1993. PROCHECK: A program to check the stereochemical quality of protein structures. *J Appl Crystallogr.*, 26(2): 283–291.

Ling B. D., Zhang L., Li X. Z., 2016. Antimicrobial resistance and drug efflux pumps in *Acinetobacter*. In: Li X. Z., Elkins C., Zgurskaya H. I. (eds) *Efflux-Mediated Antimicrobial Resistance in Bacteria.* Springer: 329–358. doi: 10.1007/978-3-319-39658-3_13.

Mittal A. K., Bhardwaj R., Mishra P., Rajput S. K., 2020. Antimicrobials misuse/overuse: Adverse effect, mechanism, challenges and strategies to combat resistance. *Open Biotechnol J.*, 14(1). doi: 10.2174/1874070702014010107.

Morris G. M., Huey R., Lindstrom W., Sanner M. F., Belew R. K., Goodsell D. S., Olson A. J., 2009. AutoDock4 and AutoDockTools4: Automated docking with selective receptor flexibility. *J Comput Chem.*, 30(16): 2785–2791.

National Center for Biotechnology Information. RND protein [*Stenotrophomonas maltophilia* K279a]. Accessed October 16, 2023. https://www.ncbi.nlm.nih.gov/protein/CAG34257.1.

Nguyen N. L., Bui V. H., Pham H. N., Dao T. T., Tran D. T., Hoang T. T., Le V. C., Pham T. N., Nguyen T. H., Pham H. Q., 2022. Ionomics and metabolomics analysis reveal the molecular mechanism of metal tolerance of *Pteris vittata* L. dominating in a mining site in Thai Nguyen province, Vietnam. *Environ Sci Pollut Res Int.*, 29(58): 87268–87280.

Nguyen T. K. O., Nguyen L., Pham N., Le D., Nguyen T., Nguyen H., Dao T., Le V., 2021. Development of a *Pteris vittata* L. compound database by widely targeted metabolomics profiling. *Biomed Chromatogr.*, 35(8): e5110. doi: 10.1002/bmc.5110.

O'Boyle N. M., Banck M., James C. A., Morley C., Vandermeersch T., Hutchison G. R., 2011. Open Babel: An open chemical toolbox. *J Cheminform.*, 3(1): 33.

Raad M., Abou Haidar M., Ibrahim R., Cheaito R., El Zakhem A., Kanj S. S., 2023. *Stenotrophomonas maltophilia* pneumonia in critical COVID-19 patients. *Sci Rep.*, 13(1): 3392.

Sánchez M. B., García-León G., Hernández A. G., Martínez J. L., 2016. Antimicrobial drug efflux pumps in *Stenotrophomonas maltophilia*. In: Li X. Z., Elkins C., Zgurskaya H. I. (eds) *Efflux-Mediated Antimicrobial Resistance in Bacteria.* Springer: 401–416. doi: 10.1007/978-3-319-39658-3_15.

Williams C. J., Headd J. J., Moriarty N. W., Prisant M. G., Videau L. L., Deis L. N., Verma V., Keedy D. A., Hintze B. J., Chen V. B., Jain S., Lewis S. M., Arendall W. B. III, Snoeyink J., Adams P. D., Lovell S. C., Richardson J. S., Richardson D. C., 2018. MolProbity: More and better reference data for improved all-atom structure validation. *Protein Sci.*, 27(1): 293–315.

Wu C.-J., Lu H.-F., Lin Y.-T., Zhang M.-S., Li L.-H., Yang T.-C., 2019. Substantial contribution of SmeDEF, SmeVWX, SmQnr, and heat shock response to fluoroquinolone resistance in clinical isolates of *Stenotrophomonas maltophilia*. *Front Microbiol.*, 10: 822.

Yamaguchi A., Nakashima R., Sakurai K., 2015. Structural basis of RND-type multidrug exporters. *Front Microbiol.*, 6: 327.

Youenou B., Favre-Bonté S., Bodilis J., Brothier E., Dubost A., Muller D., Nazaret S., Comte G., 2015. Comparative genomics of environmental and clinical *Stenotrophomonas maltophilia* strains with different antibiotic resistance profiles. *Genome Biol Evol.*, 7(9): 2484–2505. doi: 10.1093/gbe/evv161.

Appendix 1. Docking analysis. Binding energy of 8 antibiotics and 99 detected compounds in LC-qToF. (kcal/mol)

No.	Name	Binding energy (kcal/mol)
1	Trimethoprim	-9.1
2	Erythromycin	-8.33
3	Clarithromycin	-8.17
4	Ciprofloxacin	-7.8
5	Chloramphenicol	-6.5
6	Levofloxacin	-8.3
7	Tetracycline	-8.9
8	Sulfamethoxazole	-6.7
9	Evocarpine	-6.73
10	Withametelin C	-9.43
11	Hyperpapuanone	-7.5
12	Angeloylgomisin Q	-7.33
13	Belladonnine	-9.1
14	Oleoyl neocryptotanshinone	-7.27
15	Picrasinoside B	-9.07
16	Procyanidin C1	-10.7
17	Neoxanthin	-9.23
18	Esculentoside Q	-10.4
19	Stachysterone A	-8.6
20	Phytolaccagenin	-9.1
21	Methyl 12-oxooctadec-9-enoate	-5.23
22	1-Linoleoyl-3-palmitoyl-rac-glycerol	-5.23
23	Tussilagonone	-7.93
24	1,3,4,6-tetra-o-galloyl-beta-d-glucose	-8.93
25	Isoetin	-8.1
26	Sesartemin	-7.83
27	Kushenol L	-8.37
28	N-Methylcorydaldine	-6.3
29	Hispanolone	-7.5
30	Cornuside	-8.13
31	Gluroside	-7.5
32	Isotrilobine	-9.17
33	Villosolside	-8.23
34	Diosgenin-3-O-beta-D-glucopyranoside	-9.83
35	Evobioside	-10.77
36	1-(3,4-dimethoxyphenyl)-5-hydroxy-decan-3-one	-6.2
37	Dichotomoside E	-6.7
38	Embelin	-6.03
39	Mahuannin A	-9.73
40	Geissoschizine methyl ether	-8.03
41	pseudolaric acid C2	-8.37
42	Pubescene A	-8.1
43	Eupatoroxin	-8.5

No.	Name	Binding energy (kcal/mol)
44	Chenodeoxycholic acid	-8.17
45	Rhodojaponin IV	-8.3
46	Oxofangchirine	-8.87
47	Cipadesin	-8.8
48	Nimbolidin D	-11.37
49	1-(4-Hydroxybenzyl)-4-methoxy-9,10-dihydrophenanthrene-2,7-diol	-8.23
50	gibberellin A17	-7.4
51	Neobudofficide	-10.27
52	Saffloquinoside B	-8.87
53	Saikosaponin E	-11
54	Nigakihemiacetal A	-8.3
55	Ginsenoside Rh2	-9.27
56	Vitexifolin B	-6.9
57	Javanicolide C	-8.7
58	Danshenol B	-8.13
59	Hexadecyl ferulate	-5.77
60	Phanginin F	-8.6
61	L-Tetrandrine	-8.8
62	Apocarotenal	-8.17
63	Stigmasteryl ferulate	-9.27
64	Kansuiphorin B	-6.77
65	Gomphrenin I	-9.1
66	Shiromodiol diacetate	-6.47
67	Curculigosaponin B	-8.6
68	Ialibinone E	-7.57
69	Berbamine	-8.83
70	Vitamin B15	-5.6
71	Dimethylcurcumin	-7.63
72	3-O-(2'E,4'Z-decadienoyl)ingenol	-8.27
73	Cistanoside C	-8.93
74	Gibberellin A87	-8.1
75	Yadanzioside I	-9
76	Ochrolifuanine A	-9.67
77	Aspafilioside A	-10.5
78	Curculigosaponin C	-9.97
79	hymexelsin	-8.73
80	Digalactosyldiacylglycerol	-6.67
81	Cristatain	-10.47
82	Ophiopogonin D	-11.57
83	vina-ginsenoside R1	-9.47
84	Atratoglaucoside A	-10.43
85	Delphatine	-6.8
86	Gingerglycolipid B	-7.23
87	Bruceajavanone B	-9.43

No.	Name	Binding energy (kcal/mol)
88	Didymin	-9.73
89	beta-Hederin	-10.53
90	Forsythiaside	-9.10
91	Ophiopogonin B	-10
92	Iristectorene B	-6.47
93	Conyzasaponin G	-10.53
94	Dehydrobrusatol	-9.3
95	Norlobelanine	-7.63
96	Cynanchoside C2	-10.33
97	beta-Citraurin	-7.97
98	Grandoside	-7.1
99	Adouetine X	-7.7
100	Centellasaponin B	-10.37
101	Palmitoyl arucadiol	-6.53
102	Platyphylline	-8.13
103	Gancaonin U	-7.97
104	16'-Decarbomethoxy-19,20-dihydroconoduramine	-10.2
105	Echinacoside	-9.17 0
106	Albibrissinoside A	-8.27